Design Estimation of Multirotor for Heliostat Cleaning Purposes

Valentina Herrera Tchernykh
valht12@hotmail.com

Instituto Superior Técnico, Universidade de Lisboa, Portugal
January 2020

Abstract

It is becoming ever more important the automation of concentrated solar power (CSP) plants' cleaning procedures, especially for plants remotely located where it is hard for manpower to reach and maintain. At the same time, it is necessary to improve the traditional heliostat cleaning methods in order to use the least water possible avoiding methods that may damage the heliostats. The objective of the presented work is to estimate the optimal way of utilizing ultrasonic cleaning devices with multirotors for heliostat cleaning purposes.

In order to frame a strategy to understand the requirements and implications of the work required to choose a multirotor, a high-level model for an ideal multirotor was developed. The model simulates the payload capability in relation to the power required for it to make the optimal path for transporting one or several cleaning devices through a heliostat field. The work is divided in two submodels. The first submodel identifies flight-path of the multirotor and the second submodel simulates the multirotor's drive components and total weight, to find the optimal trade-off between the flying time and payload weight.
Keywords: *UAV, Multirotor, Flight-time, Payload, Heliostat, Cleaning.*

1. Introduction

As the years pass, the world continues to face more intensely the consequences of climate change not only as higher temperatures but as extreme climate phenomena as consequences of greater concentrations of greenhouse gases in the air [1]. The major cause of the greenhouse gasses is the burning of fossil fuels to use as other forms of energy, therefore, the transition to renewable energy is one of the most important matters to stop climate change. Recently, humans have developed renewable energy technologies to directly capture the sunlight and transform it into electric power with photovoltaic panels (PV) or Concentrated Solar Power (CSP) technologies. Utility scale CSP is a relative new type of solar energy and its advantages make it an essential technology to fight climate change.

2. Background

The concept of CSP is to concentrate the solar radiation on a heat transfer fluid (HTF) that is then used as the heat source to produce steam and run a turbine to generate electrical power or alternatively, the heat is simply used for industrial processes. The two most commonly used CSP technologies are the parabolic through collector technology, which uses concave mirrors to reflect the sun rays into a receiver tube, and the central receiver technology, which is a newer technology that uses slightly curved mirrors to point the sun rays into a receiver. In the central receiver plants, the mirrors reflect the sun rays to the receiver placed on top of the central tower where molten salts are used as HTF which is then stored in insulated tanks. The hot tanks provide a thermal storage which can be used when needed to produce steam and run the power block.

The problem of some renewable energy technologies such as wind and PV is that they can only produce electric power when there is wind and sun respectively whereas the electricity demand continues regardless the weather conditions. The current solution is coupling the wind farms or PVs with batteries, but they are very costly and hazardous for the environment. In the other hand, CSP plants have the great advantage of storing the solar hours in the form of thermal storage. Thanks to the thermal storage, CSP can produce dispatchable energy that results in a great advantage over PVs and other renewable energy technologies.

3. State of Art: Heliostat Cleaning Technologies

The efficiency of a CSP plant highly depends on the reflectivity of the mirrors [2], therefore it is important to maintain the mirrors clean. The fre-

quency on which the mirrors are cleaned depends on the ground and weather conditions. For example, the plants located in the north cape of South Africa aim to clean the mirrors every 7 days[1]. In other plants of the world, depending on the location, the mirrors require less or even more frequent cleaning. The most common technologies for washing the mirrors are cleaning vehicles [3]. The main disadvantage of current technologies is that they use big amounts of water that are spayed by means of a hydraulic arm attached to the vehicle. The second main disadvantage is that with slight imprecise movements, the mirrors can be damage.

CSP plants are located in high Direct Normal Irradiance (DNI) zones which are usually desertic areas where the usage of water is a problem. This is why new technologies are starting to be implemented to reduce the consumption of water. The project MinWaterCSP is investigating alternative cooling system such as Air Cooling Condensers (ACC) or hybridized cooling, as well as technologies to minimize the water used for cleaning the mirrors by recycling it [4].

Alternatively, autonomous cleaning robots are being investigated as the CSP industry looks into automizing and optimizing the operations and maintenance of the plants. For example, Figure 1 shows HECTOR, an innovative system that can alone clean the entire heliostat with the help of an operator which distributes it along the field. Its benefits have been tested and validated. Apart from using a few liters of water to clean the entire heliostat, it cleans uniformly because of its direct contact with the surface and achieves original reflectivity of the mirror even after extreme dirty conditions. Additionally, this technology is delicate and eliminates the risk of the big cleaning trucks of breaking the mirrors. Taking into account that one operator can manage several of these robots, this concept maximized the cleaning capacity per operator thus optimizes the plant's operations [5].

STERG (Solar Thermal Energy Research Group) is investigating the possibility of integrating ultrasonic cleaning system into a robot that will clean each individual mirror and will be transported around the field by means of a multirotor. ultrasonic cleaning technology consists of using ultrasonic waves that generate cavitation bubbles that agitate the liquid producing high forces on the dust adhered to the mirror. This technology consumes 600 times less water than conventional cleaning methods ($0.03\,\mathrm{L/m^2}$ of water on a horizontal surface[2]).

Figure 1: Heliostat cleaning with HECTOR at the Gemasolar solar power plant [5].

4. State of Art: UAVs Design Methods

Typically, company specific codes are used in the industry to size rotorcrafs, otherwise, at university research level, a common method found to size large gas fueled aircraft such as man driven helicopters is the fuel fraction method (R_f) [6] [7] [8]. The method, when given a mission, provides a minimum engine size and thus attempts to size other components such as rotor blades and transmissions, as well as providing a minimum gross take-off weight (GTOW) required after calculating other component weights. However, a similar method to size electric UAV drive components was not yet found to be readily available.

Magnussen [9] [10] and Dai et al. [11] address UAVs sizing using the optimization software IBM ILOG CPLEX (Cplex) in order to input the sizing variables/constraints: *Payload capacity, Dynamic performance, Flight time, Cost/complexity, Propeller RPM, Number of actuators, Propeller type, Motor type* and *Battery* (where propellers, motors and batteries are taken from datasheets) to obtain an optimal solution. Commercial solvers, such as the Cplex, outperform open source solvers since Cplex is able to optimize large scale mixed integer linear program (MILP) problems in a fast manner [12].

Other papers differentiate from optimization softwares and propose single methodologies or analytical algorithms for multirotor sizing. Gur [13] presents a multi disciplinary optimization (MDO) approach to design a propulsion system based on goals such as rate of climb and hover time, and presents a useful modeling analysis of motors and batteries as well as sensitivity analysis to certain propeller design elements. Wislow [14] identifies key driving vehicle factors implemented in a Micro Air Vehicle design tool. Starting from basic rotor

[1] This information was given to the researcher at the technical visit of a CSP plant located in the Northern Cape, South Africa

[2] This information was given to the researcher by the STERG ultrasonic cleaning system developer partner.

parameters, such as radius, solidity, and airfoil section, and an initial gross take-off weight (GTOW), a blade element momentum theory framework coupled with computational fluid dynamics (CFD) generate an estimate of rotor power and torque for a required thrust. Gatti et al. [15] propose a revised version of a classical aircraft sizing methodology, based on statistical data available in the literature, to preliminary size an electric multirotor, taking into account mission profile and a few performance requirements. Bouabdallah [3] describes a method for iteratively designing a quadrotor with a maximum mass and length to achieve a desired thrust-to-weight ratio. The method requires a database of actuator, battery, and airframe components to calculate the loop masses. Ng et al. [**?**] propose a methodology with genetic algorithms to automate the component selection, layout design and geometric sizing of small-scale quadrotors. The most suitable set of components from datasheets are selected, and organize the vehicle components/payloads, such that the resulting flight vehicle has the most compact overall size without violating any given physical or mission constraint.

In contrast of most of the above mentioned researches, Bershadsky et al. [16] and Ampatis [17] propose to parameterize drive components such as motors, batteries, propellers and ESCs to rid of the need of using databases for design and optimization. Additionally, Ampatis studies the effect of varying payload on design characteristics.

Less rigorous methods in terms of optimality of UAV design also exist. For instance, eCalc [18] is a free online tool that has become one of the most popular tools for UAV hobbyists [16]. Some researches propose this tool for multirotor design [19]. eCalc allows users to input the multirotor components and outputs a calculated flight time, in addition to other useful data. eCalc requires that the specific drive components are provided to the tool. This is one of the major differences between eCalc and the analysis algorithm described in this paper. The presented model allows users to input only payload and relevant drive system parameters instead of arbitrarily selecting specific components.

5. Methodology

An example heliostat field was chosen to simulate different flying paths with different amounts of cleaning devices per drone. The most convenient path was chosen to identify the amount of water needed per cleaning device which decides the payload weight. The identified payload was simulated with several motors selected from data-sheets with their recommended propeller and input voltage to find the best performing configuration in terms of flight-time.

To find the flight-time, a computer model was developed in MATLAB using Momentum Theory combined with Blade Element Theory to simulate the Thrust, Power and Torque of a multirotor with a set number of rotors a specific battery size and correspondent total weight. The model was validated by comparing the results with commercial data.

5.1. Aerodynamics: Momentum Theory

Momentum theory uses the fundamental laws of fluid mechanics (conservation of mass, energy and momentum), to relate the inflow and outflow of the propeller's plane to its thrust and power. The model is useful to understand the global mechanism of the rotor including the limits for an ideal performance and the induced power requirements, but it is not enough to physically design a propeller since it does not relate to the loads or flow around the blades [20].

To use momentum theory, the rotor is assumed to be a disk of infinite amount of blades which adds momentum and energy to the air flow. The rotor can accelerate the air flow downstream thanks to the pressure difference that it can support across it as shown in Figure 2, in this way produces thrust in the opposite direction of the downstream air.

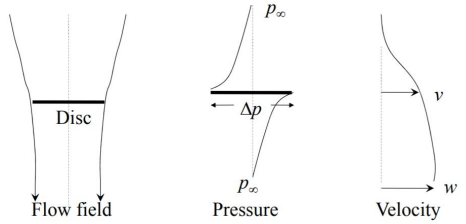

Figure 2: Flow pressure and velocity across the rotor disk [20].

Figure 2 shows the axial inflow velocity V which the rotor experiences during horizontal or vertical flight where V is the velocity at which the rotor is moving, v is the induced velocity of the air generated by the rotor and w is the wake or induced velocity at far downstream.

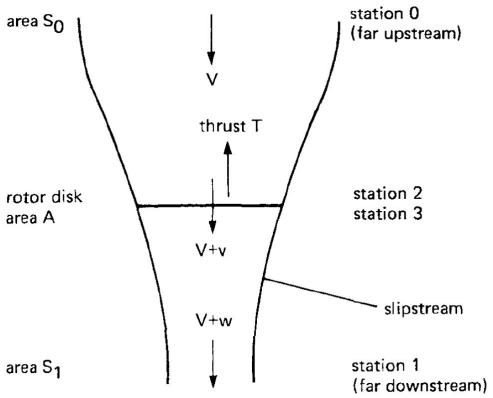

Figure 3: Momentum theory flow model [21].

From conservation of momentum, the thrust

generated at Station 2 is:

$$T = \dot{m}(V + w) - \dot{m}V = \dot{m}w \tag{1}$$

From conservation of energy, the work generated at Station 2 is:

$$T(V + v) = \frac{1}{2}\dot{m}w(2V + w) \tag{2}$$

Solving for the induced wake $T/\dot{m}$ in Eq. (1) and Eq. (2) results in $w = 2v$. Therefore,thrust can then be expressed as:

$$T = \dot{m}w = 2\rho A(V + v)v \tag{3}$$

At hover conditions the rotor has no forward or vertical speed so $V = 0$. Thus, induced velocity at hover can be expressed as:

$$v_{\mathrm{h}} = \sqrt{\frac{T}{2\rho A}} \tag{4}$$

Finally, the ideal induced power required to hover can then be determined for a given thrust:

$$P = Tv = T\sqrt{\frac{T}{2\rho A}} \tag{5}$$

5.2. Blade Element Theory

Blade Element Theory comes closer to the blade's reality unlike Momentum Theory that considers the propeller as a disk composed of infinite amount of blades, and who's surface produces a pressure jump. Blade Element Theory is used to calculate the interaction with the fluid over each section of the blade which then is integrated to find the resultant forces over the entire blade [22].

Figure 4 is the top view of a rotor where R is the radius, y is the radial length ($y = 0$ at the hub and $y = R$ at the tip), c is the blade's cord, Ω is the angular velocity and ΩR is the tangential velocity.

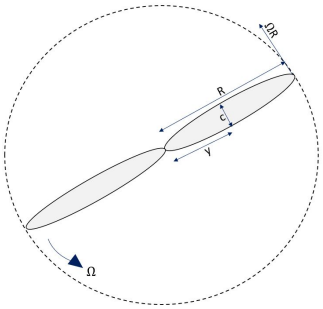

Figure 4: Blade section top view.

Figures 5 is the profile view of a blade. The blade section pitch, θ, is measured between the plane of rotation and the zero lift line. The aerodynamic angle of attack, α, is measure between the resultant

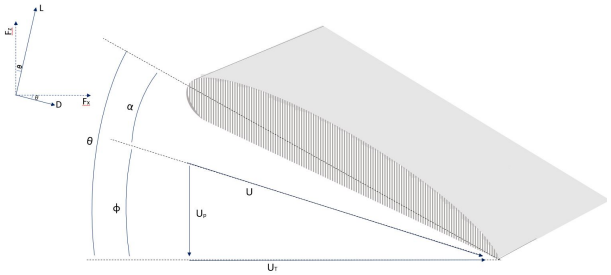

Figure 5: Blade cross-section.

air velocity seen by the blade, U, and the zero lift line and can be expressed as $\alpha = \theta - \phi$. U has a tangential component, $U_T = \omega y$, and a perpendicular component, $U_P = V + v$.

The resultant velocity inflow angle can be given by:

$$\phi = arctan\left(\frac{U_{\mathrm{P}}}{U_{\mathrm{T}}}\right)$$

The rotor inflow ratio, λ, defined as the ration of the total inflow velocity to the rotor tip speed $\lambda = (V+v)/(\Omega R)$ (the inverse of tip speed ratio for wind turbines). Inflow ratio at hover can be written in terms of thrust and angular velocity:

$$\lambda_{\mathrm{h}} = \frac{\sqrt{\frac{T}{2\rho A}}}{\Omega R} \tag{6}$$

The section lift force, L, and drag force, D, act normal and parallel to the resultant velocity vector, U, respectively. The section lift and drag forces are expressed as:

$$L = 1/2c\rho U^2 c_l \tag{7}$$
$$D = 1/2c\rho U^2 c_d \tag{8}$$

where c is the blade chord, ρ is the air density and c_L and c_D are the section lift and drag coefficients respectively.

c_l and c_d are complicated functions of the angle of attack, α. To simplify calculation of c_l, the stall and compressible effects are assumed to be negligible so that c_l can be expressed as a linear relationship between the section lift coefficient and the angle of attack, $c_l = a\alpha$ [23], where a is the slope of the blade two-dimensional lift curve and is denoted by $a = 5.7$ as a typical value used in literature [21].

From the diagram on the top left corner of Figure 5. The force acting on the x and z direction of the blade are given by:

$$F_z = Lcos(\phi) - Dsin(\phi) \tag{9}$$
$$F_x = Lsin(\phi) - Dcos(\phi) \tag{10}$$

Defining the differential thrust, torque and power with the acting forces on the blade section for all the blades, N, of the rotor results in:

$$dT = NF_z dr \tag{11}$$

$$dQ = NF_x r dr \quad (12)$$
$$dP = \Omega dQ = \Omega N F_x r dr \quad (13)$$

The total forces on the propeller are obtained by integrating from the root to the tip of the blades.

It is assumed that the rotor has a low disk loading, meaning the inflow velocity of λ is small compared to the rotational speed, and consequently, U_P/U_T is also small. This is a reasonable assumption as the rotor operates at high angular velocities. Therefore, small angle assumption, $\phi = arctan(U_P/U_T) \ll 1$, is applicable to the propeller of a multirotor and it approximates $\phi \simeq U_P/U_T$, $cos(\phi) \simeq 1$ and $sin(\phi) \simeq \phi$.

Defining as coefficients the ratios between the actual thrust, torque and power obtained from the propeller and the respective ideal that the air would have over the entire disk area and angular velocity, results in:

$$C_T = T/[\rho A(\Omega R)^2] \quad (14)$$
$$C_Q = Q/[\rho A(\Omega R)^2 R] \quad (15)$$
$$C_P = P/[\rho A(\Omega R)^3] \quad (16)$$

Therefore, $C_P = C_Q$ as a consequence of Eq. (13) and, by applying small angle assumption to Eq. (11), the differential C_T can be explained as

$$dC_T = \frac{\sigma a}{2}(\theta r^2 - \lambda r)dr \quad (17)$$
$$\text{with}$$
$$\sigma = \tfrac{N}{\pi R^2}\int_0^R c(r)dr$$

Where $r = y/R$ and represents a dimensionless radial location on the blade, measured from the hub, $r = 0$, to the blade tip, $r = 1$. From the definition of U_p and U_t; $U_p/U_t = (V + v)/\Omega y = \lambda(R/y)$.

For a blade with ideal distribution, $\theta = \theta_t/r$ [21] where θ_t is the pitch angle at the tip of the blade Solving Eq. (17) for an ideal distributed blade results in:

$$C_T = \frac{\sigma a}{4}\alpha_t \quad (18)$$

From Eq. (6) and Eq. (14) the rotor inflow ratio at hover can be expressed in terms of C_T.

$$\lambda_h = \sqrt{\frac{C_T}{2}} \quad (19)$$

Substituting Eq. 16 with C_t and λ_h results in:

$$C_P = C_T\lambda = \frac{C_T^{\frac{3}{2}}}{\sqrt{2}} \quad (20)$$

The C_P for an ideal blade only represents the induced power loss. A real blade has also profile losses and additional losses due to nonuniform inflow, swirl in the wake and tip losses.

From Figure 5, $\theta = \alpha + \phi$ therefore,

$$\theta_t = \frac{4C_T}{\sigma a} + \lambda \quad (21)$$

Solving for the rotor inflow ratio results in:

$$\lambda = -\frac{\sigma a}{8} + \frac{1}{2}\sqrt{\left(\frac{\sigma a}{8}\right)^2 + 4\frac{\sigma a}{8}\theta_t} \quad (22)$$

5.3. Figure of Merit

Figure of merit is defined as the ideal power loss over the actual power loss of the propeller.

$$M = \frac{P_{\text{ideal}}}{P} = \frac{T\sqrt{\frac{T}{2\rho A}}}{P} \quad (23)$$

According to literature, at the design loading of the rotor, the typical figure of merit, M, lays in between 0.55 and 0.60 [21]. $M = 0.6$ was used in the model below to estimate the real performance of a propeller.

6. Model

The model is divided into two submodels that depend on each other's outputs to define their inputs.

The first submodel is the Flight-Path Model which creates an example heliostat field where different flying paths are simulated with different amounts of cleaning devices per multirotor. The model is scalable in terms of the size of the field, number of heliostats and mirror dimensions. Figure 6 displays the example field chosen for this work consisting of 540 heliostats with mirrors of 2.23 m^2. In Figure 6 the red dot represents the receiver tower, the black squares represent the heliostats and the blue triangles are the pedestals structure that joins 6 heliostats together. Such a system is referred to as HelioPod[3].

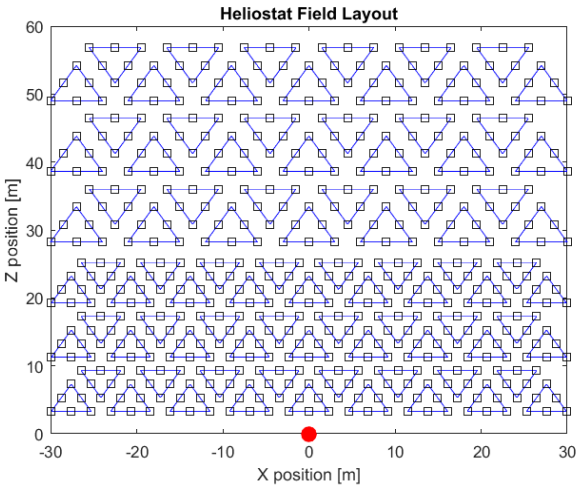

Figure 6: Example field with 540 heliostats.

The path accomplished in the least amount of time and also requiring the least airborne and idle time for the multirotor is chosen to identify the main design requirements of the multirotor and cleaning device.

[3]HelioPod was developed and demonstrated at STERG [24].

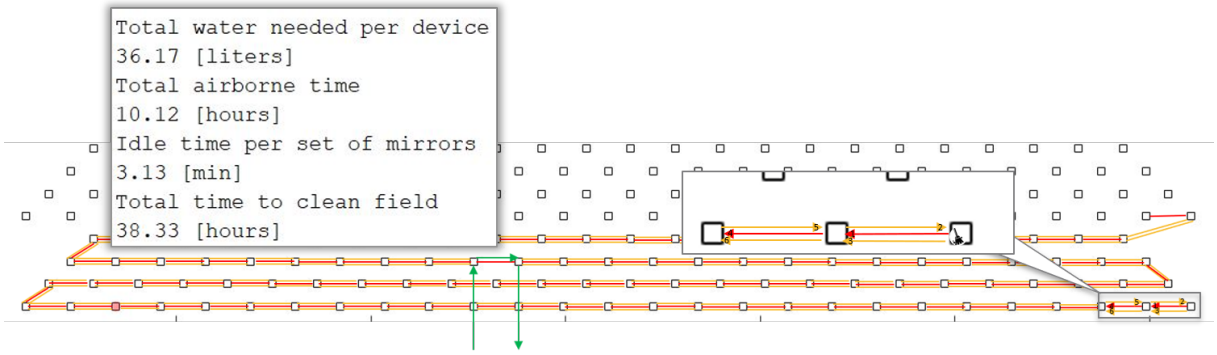

Figure 7: Layout and resulting outputs of 1 drone and 4 devices for Central Station scenario.

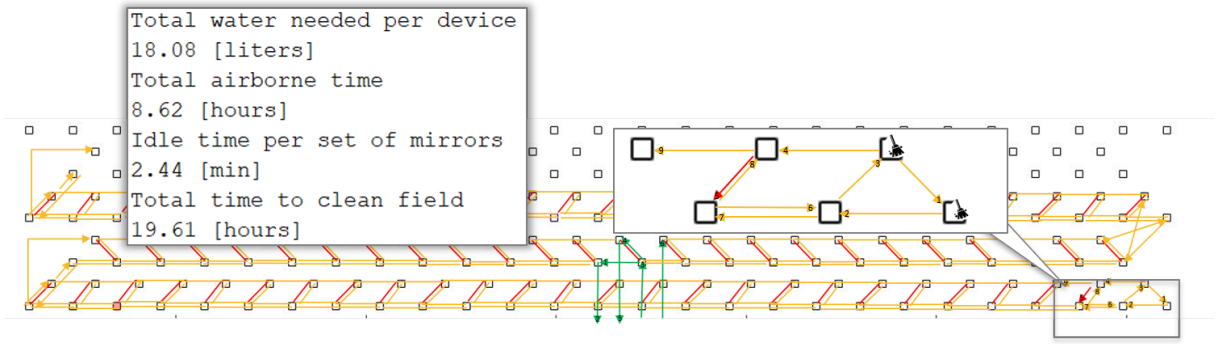

Figure 8: Layout and resulting outputs of 1 drone and 2 devices for Central Station scenario.

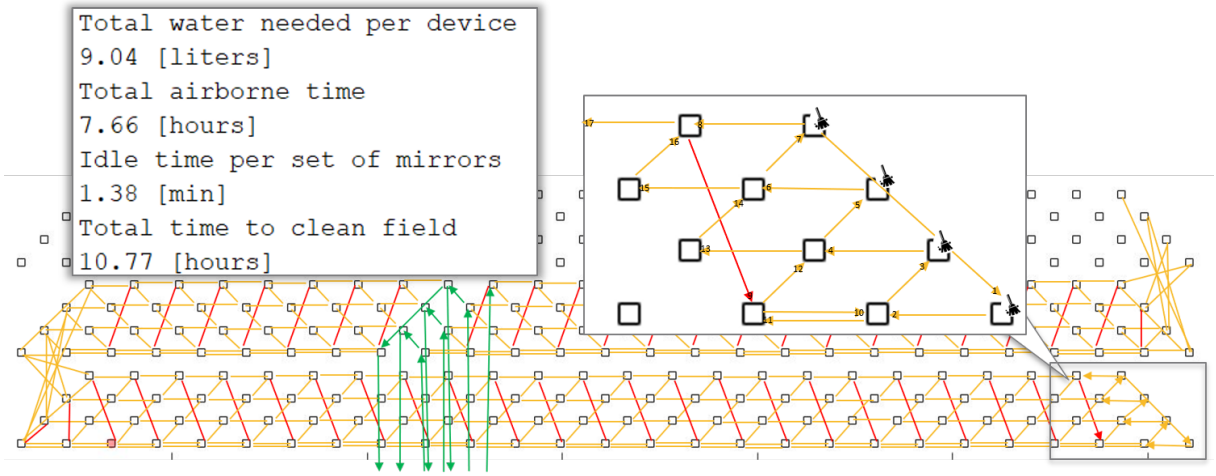

Figure 9: Layout and resulting outputs of 1 drone and 4 devices for Central Station scenario.

Two scenarios where considered for the Flight-Path model: (1) Central Station scenario where the multirotor returns to a central point to refill the water of the cleaning devices and (2) the Cart scenario where a self driven cart transport the water and provides docking spot for the multirotor. In the presented work, the amount of water fitted into the cleaning device needs to be identified to then be given to the cleaning device manufacturer. The weight of the water plus the cleaning device would equal the weight of the multirotor's payload.

The bottleneck of the flight-path is the amount of time that it takes the device to clean each mirror (3.6 min). Assigning more devices to the same drone alleviates the bottleneck although the path sketch gets more complicated. It is desired to utilize the drone as much as possible avoiding it to be idle, but at the same time,never allowing the devices to wait for the drone to pick them up since this situation would add to the bottleneck. To avoid this to happen, it is appointed a buffer time of 1 minute for the drone to wait.

Figures 7, 8 and 9 show the paths with the flying, docking and recharging sketch for one drone carrying one, two and four devices respectively in the Central Station scenario. More than 4 devices

was not further considered since the fifth device resulted on a waiting time of less than the 1 minute required buffer. The yellow lines represent the flight trajectory to pick up and place the cleaning devices, the red lines represent the flight trajectory to dock, the green lines represent the flight trajectories to refill and water, and the box displays the outputs of the respective layout.

The weight of the payload is used in the second submodel, the Multirotor Sizing Model, to be simulated with several motors taken from the data sheets of the drone motor manufacturer, *T-motor*. 100 different motors where selected with the suggested propeller and input voltage and each was simulated with 50 different battery sizes plus the selected payload to obtain the flight-time. The configuration with the longest average flight-time is then chosen as the reference multirotor configuration.

In the last part of the multirotor Sizing model, the reference configuration is modeled with a selected range of propeller and battery sizes to identify the resulting flight-times and other parameters such as torque which relates to the inertia and the maneuverability of the multirotor. According to the outputs the user can choose the most suitable multirotor configuration with a resulting design flight-time.

Figure 10 is the summary of the model's flow chart where yellow belongs to the Flight-Path model and green belongs to the multirotor Sizing model.

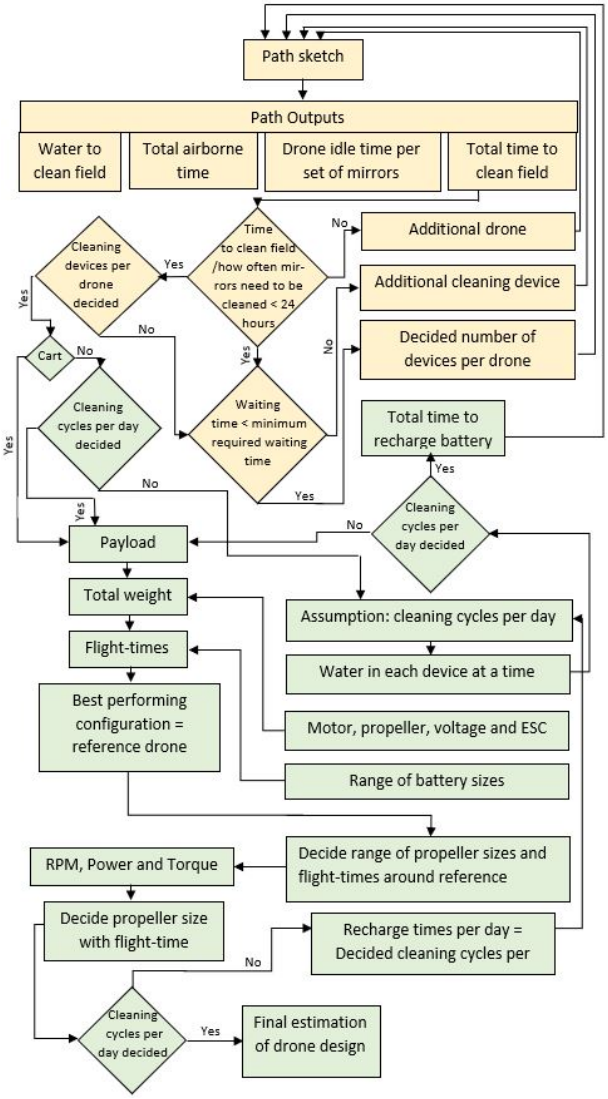

Figure 10: Model's flowchart.

7. Results & Discussion

The results of the submodels are summarized separately in the following subsections.

7.1. Flight-Path Model

The selected path was with four devices per multirotor in *zig-zag* pattern for both, Base Station scenario and Cart scenario as shown in Figure 9. 4 cleaning devices maintain the multirotor as occupied as possible and still leave $1\,\mathrm{min}$ buffer while the multirotor waits the cleaning devices to finish their respective mirror.

The purpose of the path modeling is to estimate the required payload of the multirotor, which directly depends on the amount of water fitted into each device. Since the multirotor flies longer as the payload is lighter, the optimal minimum amount of water to fill into the device any time must be identified.

The Cart scenario has the availability to refill the water at any point in the cleaning process whereas the Base Station scenario has to match the multirotor's battery recharging. Therefore for the Cart scenario two settings were modeled, one where $1\,\mathrm{L}$ of water is fitted into the device and another where $0.5\,\mathrm{L}$ are fitted. Comparing the two scenarios allows to see the advantages of reducing the weight of the water to be carried versus the extra flight time to recharge the cleaning devices more often. It is concluded that it is favorable to decrease the quantity of water so the decided amount of water to be fitted into the devices of the Cart scenario is $0.5\,\mathrm{L}$ of water.

For the Central Station scenario, it is necessary to understand the operational requirements of the field in terms of how often the mirrors need to be cleaned. Generally, the heliostats in the CSP plants located in the Northern Cape of South Africa are expected to be cleaned every 7 days. Dividing the entire field's cleaning job into 7 days would mean that $1.3\,\mathrm{L}$ of water would be used per cleaning device per day. If the total time required to clean the field divided by how often the mirrors should be cleaned is more than 24 hours it is required to add an additional multirotor. For the example case, 1 multirotor is enough to compile with the cleaning

requirements.

To optimize the flight-path of the multirotor, the water refilling is matched with the recharging of the multirotor's battery. At this point, the flight-time of the multirotor is unknown. Once the flight-time is known the airborne time per day is divided into the flight-time to obtain the recharge times per day which equal the cleaning cycles per day. The 1.3 L of water will then be divided into the cleaning cycles to obtain the amount of water fitted into the device.

7.2. Multirotor Sizing Model

The first assumption of water fitted into the device is 1 L, plus 2 kg of the cleaning device it self, results in a payload of 3 kg. The payload is then modeled with all the configurations from the datasheets and batteries, and the best resulting configuration as chosen as reference.

The combination of the reference motor with the reference ESC is modeled with 7 propellers sizes (reference propeller $\pm$ 3 in) and 50 different 12S battery sizes from 2000 mAh to 5000 mAh. The resulting behavior is provided in the Figure 11, which shows that the bigger the propeller, the longer resulting flight-time.

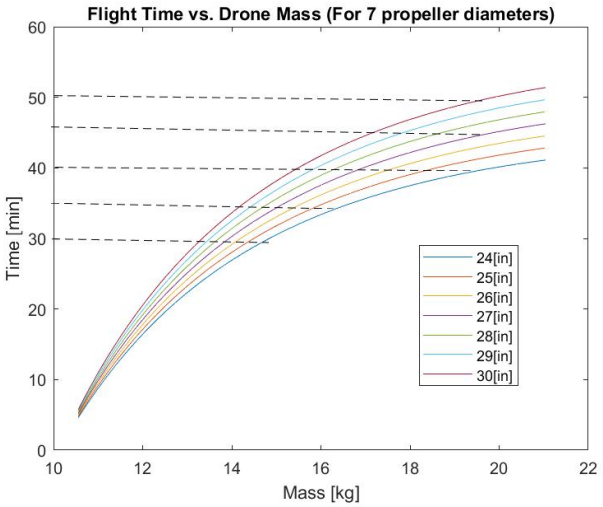

Figure 11: 7.5 kg multirotor plus 3 kg Payload and 12S LiPo batteries from 2000 mAh to 50000 mAh. Dashed lines indicated 50, 45, 40, 35, and 30 min flight-time

A bigger propeller is not always better because of the increase in torque which limits the fast response of the multirotor and therefore compromises the maneuverability. In addition, the current needed to start, stop or slow down the propeller can overheat the motor by exceeding its peak current.

The highest theoretical flight-time achieved with the range of batteries is 51 min and states the reference from which lower flight-times are chosen to evaluate the correspondent multirotor configuration, each with a range of propellers. 50, 45, 40, 35, and 30 min of flight-time is inserted into the model and the results are compared. Additionally, the power needed to take-off and stop the propellers of each multirotor combinations is considered to see if it is over or under the peak current of the motor. Only the combinations within a safety margin under the peak current are selected and the one with longest flight-time will be chosen as multirotor configuration.

In the example case, the power to take-off or stop the propellers was not calculated. From the first iteration of the model, the required flight time per day is 1.09 h. A 1 h flight-time multirotor is hardly achieved and, from the longest reference flight-time of 51 min, it was understood that the multirotor's battery should be recharged at least one time per day which means that the design flight-time of the multirotor should be 33 min plus a margin for the extra power required to take-off. This assumptions results in 2 cleaning cycles per day meaning that for the Central Station scenario, the cleaning devices should each carry 0.65 L of water per cycle. A safety margin of 0.15 L of water is added in case of any leakage resulting in a total of 0.80 L of water to fit in each device. The initial assumption of 1 L is readjusted to 0.80 L and the battery charging time of 1 h is added to the Path Model. Results are displayed in Table 1.

Table 1: Results for multirotor's path in Central Station scenario with 4 cleaning devices carrying 0.8 L of water each.

Total airborne time	7 h 52 min
Idle time per set of mirrors	1.38 min
Total time to clean field	17 h 58 min

The total airborne time slightly increased since the water has to be refilled more often. In the other hand, the total time to clean the field significantly increased after 1 h a day was added to charge the battery. 17.96 h of cleaning are easily achieved in 7 days and therefore, nothing is further iterated for this constrain.

In the Cart scenario the multirotor should also recharge the battery at least one time per day given that it has 1.04 h of flight-time a day. Table 2 shows the final results for the Cart scenario after adding the total of 7 h of battery charging time and extra flight-time to recharging station.

Table 2: Results for multirotor's path in Cart scenario with 4 cleaning devices carrying 0.5 L of water each.

Total airborne time	7 h 18 min
Idle time per set of mirrors	1 min 23 s
Total time to clean field	17 h 24 min

Table 3: Specification of 7 multirotor configurations designed for 40 min flight-time and 2.8 kg payload.

Flight-Time: 40 min

Diameter_in	pitch_in	Batt_Energy_mAh	Batt_Weight_g	AUW_g	RPM	Power_W	Torque_Nm
24	7.7	45000	11080	19943	4189	673	1.29
25	8.1	39000	9770	18633	3706	584	1.27
26	8.4	35000	8897	17760	3352	522	1.25
27	8.7	32000	8242	17105	3056	475	1.25
28	9	29000	7587	16450	2791	432	1.25
29	9.4	27000	7151	16014	2552	401	1.27
30	9.7	25000	6714	15577	2356	372	1.27

The above identified flight-time is 33 min. Adding a margin which accounts for the extra energy to take-off and maneuver the multirotor results in 40 min. Table 3 displays the multirotor configurations for the selected flight-time and payload.

For the chosen motor, the manufacturer suggests 26, 27 or 28 in propellers. For the purposes of the multirotor and the relative low payload, it is reasonable to consider bigger propeller sizes than the suggested ones, to achieve longer flight-times. However, their suitability should be verified with the technical specifications of the motor or experimentally. Since the technical limitations of the motor were not measured in this research, the manufacturer suggestions are considered and the 28 in propellers is chosen because achieves the same 40 min flight-time with smaller battery which results in less weight and more operation flexibility.

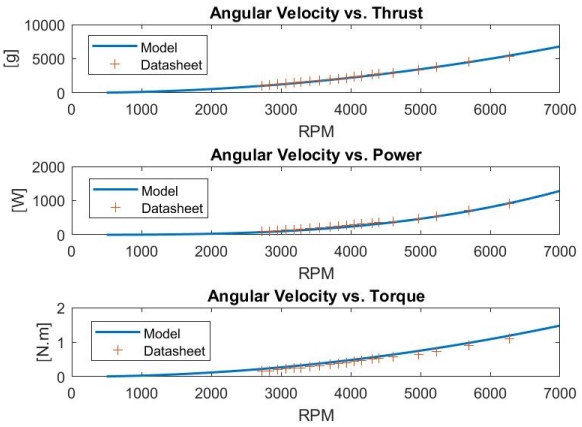

Figure 12: Thrust, Power and Torque of motor MN505 KV320 with propeller 20 in×6 in found at T-Motor.

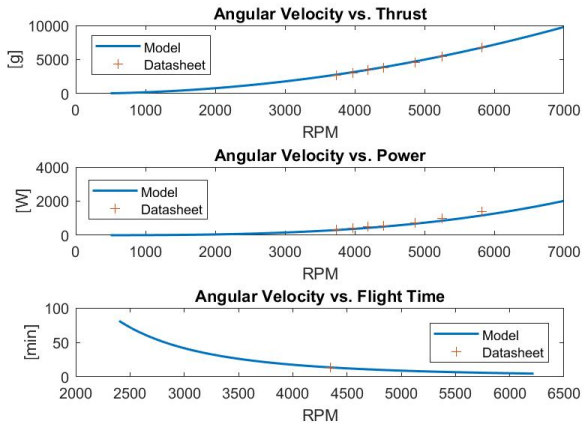

Figure 13: Thrust, Power and Flight-time of motor P80 KV170 with propeller 30 in×10.5 in found at T-motor

8. Validation

To validate the model, six motors plus propellers where chosen from the data-sheets of T-Motor and plotted on top to the graphs generated by the model that simulate, thrust, power, torque and flight-time given the RPM and propeller specifications. Figure 12 and 13 display two out of the six motors used for validation.

The thrust, power and torque of the samples closely follow the model's graphs. The flight-time for smaller propellers is also closely estimated whereas for bigger propellers the model gives slightly higher flight-times since the model only considers hover while the flight-time specification of the manufacturer also considers take-off and maneuverability which requires higher power for bigger propellers.

9. Conclusion

The developed model framed a strategy to identify the required characteristics of a multirotor whose purpose is to transport one or several cleaning devices through a CSP heliostat field. It is concluded that the model is a suitable high-level estimation for choosing a multirotor with the above mentioned purposes.

The model concludes that for a field of 540 heliostats with mirrors of 2.23 m^2, a quadcopter should carry 4 cleaning devices parallel. If the field holds a cart, each cleaning device should be refilled with 0.5 L of water. If the drone needs to come back to the central station, the devices should be refilled with 0.8 L of water. The total time to clean the field with no cart is 17 h and 57 min. For such a heliostat field size the addition of a cart is not justified.

A drone with 28 in propeller size and a 28 000 mAh battery with hover flight-time of 40 min will carry a 2.8 kg cleaning device at a time. The drone will do two cleaning cycles per day. It will recharge the battery before initiating the first cycles and in between cycles.

The concluding results show that the model is able to frame a strategy for selecting a multirotor and its flying sketch. Future work should be done on investigating the advantages of utilizing a hexacopter or hectocopter instead of quadcopter. Furthermore, the impact of airflow generated by the multirotor should be considered to understand the impact on the cleaning system. Lastly, weather condition limitations should be added to the model to identify additional constraints.

References

[1] EPA. Sources of Greenhouse Gas Emissions. *Climate Change*, pages 1–2, 2015.

[2] Ahmed Alami Merrouni, Ahmed Mezrhab, Abdellatif Ghennioui, and Zakaria Naimi. Measurement, comparison and monitoring of solar mirror's specular reflectivity using two different reflectometers. *Energy Procedia*, 119:433–445, 2017.

[3] Sahar Bouaddi, Aránzazu Fernández-García, Chris Sansom, Jon Ander Sarasua, Fabian Wolfertstetter, Hicham Bouzekri, Florian Sutter, and Itiziar Azpitarte. A review of conventional and innovative-sustainable methods for cleaning reflectors in concentrating solar power plants. *Sustainability*, 10(11):3937, 2018.

[4] Reduction of water consumption in concentrated solar power (csp) plants. https://www.minwatercsp.eu. Accessed: 2019-06-30.

[5] Michael Hardt, Daniel Martínez, Antonio González, Candido Garrido, Sergio Aladren, José Ramón Villa, and Jaime Saenz. HECTOR – heliostat cleaning team-oriented robot. *SolarPaces Conference*, (November 2011), 2011.

[6] Adeel S Khalid. *Development and implementation of rotorcraft preliminary design methodology using multidisciplinary design optimization*. PhD thesis, Georgia Institute of Technology, 2006.

[7] Daniel P Schrage. Teaching graduate rotorcraft design based on twenty years of experience. *age*, 10:1, 2005.

[8] Joseph Hutson Davis. *Design methodology for developing concept independent rotorcraft analysis and design software*. PhD thesis, Georgia Institute of Technology, 2007.

[9] Øyvind Magnussen, Geir Hovland, and Morten Ottestad. Multicopter uav design optimization. In *2014 IEEE/ASME 10th International Conference on Mechatronic and Embedded Systems and Applications (MESA)*, pages 1–6. IEEE, 2014.

[10] Øyvind Magnussen, Morten Ottestad, and Geir Hovland. Multicopter design optimization and validation. 2015.

[11] Xunhua Dai, Quan Quan, and Kai-Yuan Cai. Design automation and optimization methodology for electric multicopter uavs. *arXiv preprint arXiv:1908.06301*, 2019.

[12] Bernhard Meindl and Matthias Templ. Analysis of commercial and free and open source solvers for linear optimization problems. *Eurostat and Statistics Netherlands within the project ESSnet on common tools and harmonised methodology for SDC in the ESS*, 20, 2012.

[13] Ohad Gur and Aviv Rosen. Optimizing electric propulsion systems for uavs. In *12th AIAA/ISSMO Multidisciplinary Analysis and Optimization Conference*, page 5916, 2008.

[14] Justin M Winslow, Vikram Hrishikeshavan, and Inderjit Chopra. Design methodology for small scale unmanned quadrotors. In *55th AIAA Aerospace Sciences Meeting*, page 0014, 2017.

[15] Mauro Gatti, Fabrizio Giulietti, and Matteo Turci. Maximum endurance for battery-powered rotary-wing aircraft. *Aerospace Science and Technology*, 45:174–179, 2015.

[16] Dmitry Bershadsky, Steve Haviland, and Eric N Johnson. Electric multirotor uav propulsion system sizing for performance prediction and design optimization. In *57th AIAA/ASCE/AHS/ASC Structures, Structural Dynamics, and Materials Conference*, page 0581, 2016.

[17] Christos Ampatis and Evangelos Papadopoulos. Parametric design and optimization of multi-rotor aerial vehicles. In *Applications of Mathematics and Informatics in Science and Engineering*, pages 1–25. Springer, 2014.

[18] ecalc. https://www.ecalc.ch/xcoptercalc.php. Accessed: 2019-09-30.

[19] Juan Alberto Benito, Guillermo Glez-de Rivera, Javier Garrido, and Roberto Ponticelli. Design considerations of a small uav platform carrying medium payloads. In *Design of Circuits and Integrated Systems*, pages 1–6. IEEE, 2014.

[20] Volker Bertram and Volker Bertram. Chapter 2 – Propellers. In *Practical Ship Hydrodynamics*, pages 41–72. Butterworth-Heinemann, jan 2012.

[21] W Johnson. Helicopter theory, 1994. *Dover Publications*, 1994.

[22] KM Palanduz. Experimental Analysis of a Variable Pitch Multi-rotor Propeller. (October), 2017.

[23] J Seddon and S Newman. Basic helicopter aerodynamics, american institute of aeronautics and astronautics. *Inc., Reston, VA*, 2001.

[24] Helio100. https://helio100.sun.ac.za/. Accessed: 2019-09-30.